

Electron demagnetization in asymmetric magnetic reconnection

C. Norgren^{1,2}, D. B. Graham¹, Yu. V. Khotyaintsev¹, M. André¹, A. Vaivads¹, L.-J. Chen³, P.-A. Lindqvist⁴, G. T. Marklund⁴, R. E. Ergun⁵, W. Magnes⁶, R. J. Strangeway⁷, C. T. Russell⁷, R. B. Torbert⁸, W. R. Paterson⁹, D. J. Gershman^{3,9}, J. C. Dorelli³, L. A. Avanov³, B. Lavraud¹⁰, Y. Saito¹¹, B. L. Giles⁸, C. J. Pollock⁸, and J. L. Burch¹²

(1) Swedish Institute of Space Physics, Uppsala, Sweden. (2) Department of Physics and Astronomy, Uppsala University, Uppsala, Sweden. (3) NASA Goddard Space Flight Center, Greenbelt, MD, USA. (4) KTH Royal Institute of Technology, Stockholm, Sweden. (5) Laboratory of Atmospheric and Space Physics, University of Colorado, Boulder, CO, USA. (6) Space Research Institute, Austrian Academy of Sciences, Graz, Austria. (7) University of California, Los Angeles, CA, USA. (8) University of New Hampshire, Durham, NH, USA. (9) University of Maryland, College Park, MD, USA. (10) IRAP, CNRS, Toulouse, France. (11) Institute of Space and Astronautical Science, JAXA, Sagami-hara, Japan. (12) Southwest Research Institute, San Antonio, TX, USA.



Introduction

Inside the electron diffusion region (EDR) of magnetic reconnection, the electron gyroradius ρ_e can become comparable to the length scales of the magnetic field curvature and of changes in plasma temperature and density. When this happens, the guiding center theory for electron motion breaks down - the electron motion becomes complicated, following meandering trajectories - allowing finite gyroradius effects and mixing of plasmas of different character.

How finite gyroradius effects and electron demagnetization manifest in reconnection in nature has hitherto been challenging to study, due to the small length and time scales involved. We study these effects at a magnetopause crossing (16 October 2015, 10:33:24-10:33:32) where the four spacecraft of the Magnetospheric Multiscale (MMS) mission pass close to, or inside, the EDR and observe agyrotropic electron distributions consisting of a core with $T_{\parallel} > T_{\perp}$, and a crescent with $T_{\perp} > T_{\parallel}$. Figure 1 shows an overview of the event.

Topology of reconnecting current layer

MMS pass through the magnetospheric inflow ($v_L > 0$, $B_M > 0$, $T_{\parallel} > T_{\perp}$), electron reconnection outflow ($v_L < 0$, $B_M < 0$), and magnetosheath inflow ($v_L > 0$) below the X line (Figures 1, 2 and 3).

In these regions, $\mathbf{E}' = \mathbf{E} + \mathbf{v}_e \times \mathbf{B}$ is sufficiently large that the electrons are no longer frozen-in to the magnetic field (Figure 2k). This non-ideal electric field is approximately balanced by the pressure divergence term: $|\mathbf{E} + \mathbf{v}_e \times \mathbf{B} + \frac{\nabla \cdot \mathbf{P}_e}{n_e e}|_N \lesssim 1$ mV/m (Figure 1j).

The four spacecraft observe slightly different signatures, which allows us to characterize the size and orientation of the boundaries (Figures 2 and 3c). The magnetosphere and magnetosheath boundaries separating the two inflow regions from the outflow are at an angle 34° , indicating a rapidly narrowing (widening) current sheet toward (away from) the X line. MMS1 observed the narrowest jet ~ 0.25 s ($\sim 10:33:30.5$), $w \sim 15$ km $\sim 10\rho_e$. The structure of the electron flow in the outflow region and magnetosheath inflow is illustrated in Figure 3c. The direct passage from outflow to inflow indicates MMS is close to the EDR (Figures 2i and 3b).

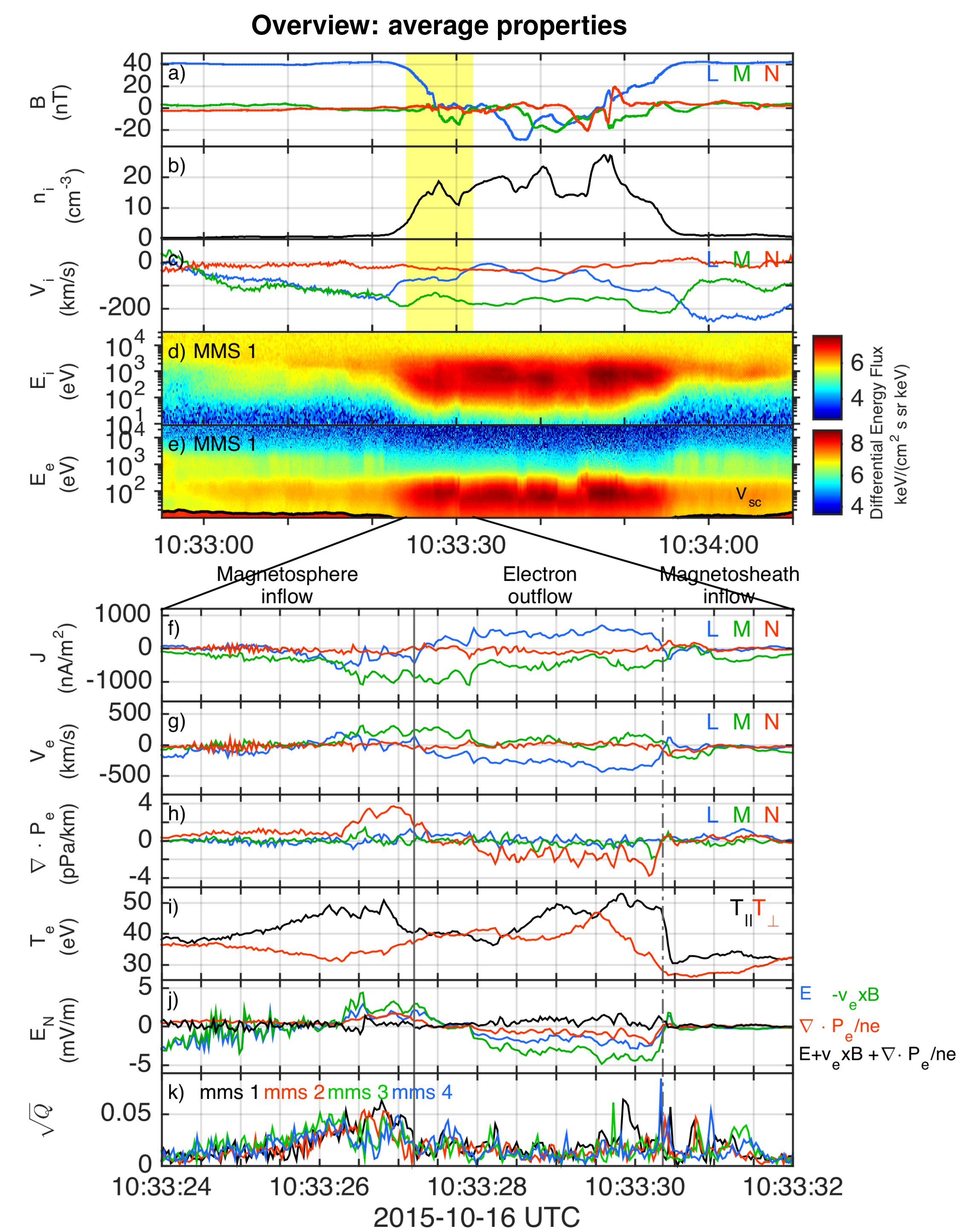


Figure 1: MMS make an outbound and inbound crossing of the magnetopause. (a) Magnetic field. (b) Density. (c) Ion velocity. (d) Omnidirectional electron differential energy flux. (e) Omnidirectional ion differential energy flux. (f) Current density. (g) Current density J_M derived from electron and ion moments. (h) Electron velocity parallel to \mathbf{B} . (i) Perpendicular electron velocity $v_{\perp,L}$. (j) Electric field E_N . (k) Electric field in the electron bulk frame, $E'_N = E_N + (\mathbf{v}_e \times \mathbf{B})_N$. (l) Electron frame energy dissipation, $\mathbf{E}' \cdot \mathbf{J}$.

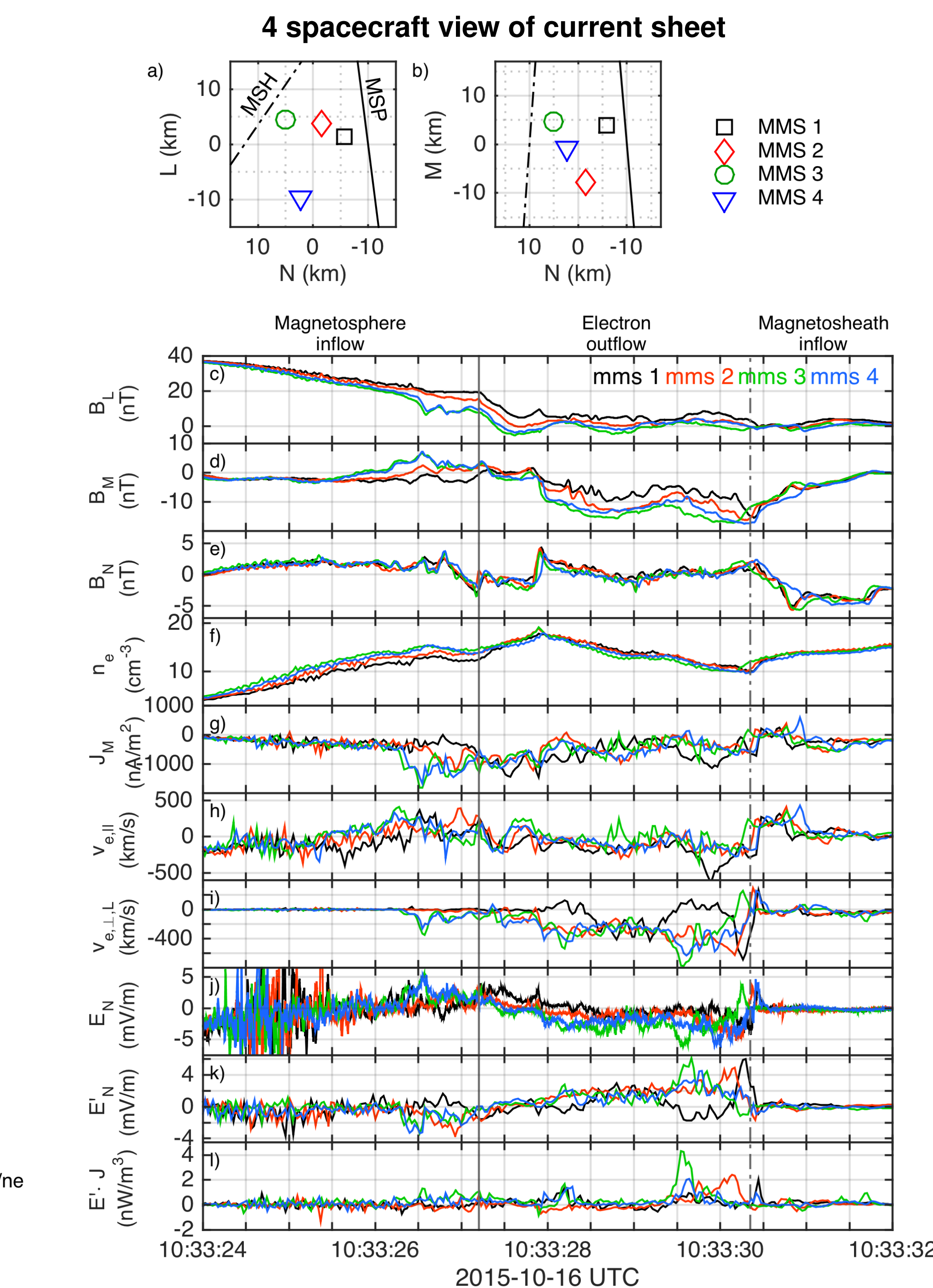


Figure 2: Detailed structure of current sheet as seen by the four spacecraft. Spacecraft configuration in a) N-L plane and b) N-M plane. The black solid and dashed lines indicate the magnetosphere and magnetosheath boundary orientation, respectively, obtained from timing analysis. Magnetic field c) B_L d) B_M and e) B_N . f) Electron density. g) Current density J_M derived from electron and ion moments. h) Electron velocity parallel to \mathbf{B} . i) Perpendicular electron velocity $v_{\perp,L}$. j) Electric field E_N . k) Electric field in the electron bulk frame, $E'_N = E_N + (\mathbf{v}_e \times \mathbf{B})_N$. l) Electron frame energy dissipation, $\mathbf{E}' \cdot \mathbf{J}$.

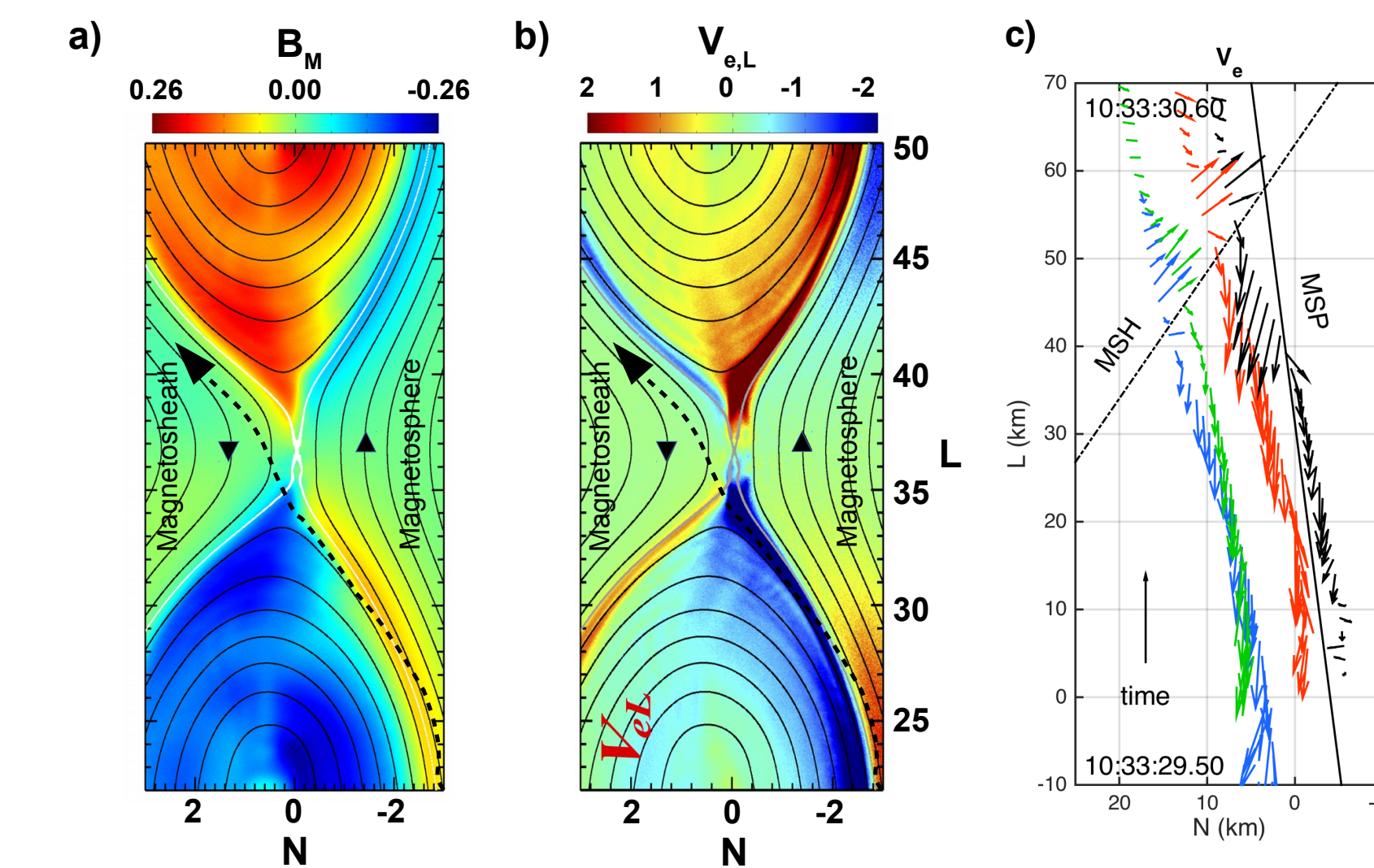


Figure 3: Illustration of spacecraft trajectory (dashed line in panels a and b) through an asymmetric reconnection layer. The figures in a-b) are from the simulation by Chen et al. [2016], and we refer to this paper for further descriptions. The distances are given in ion inertial lengths, d_i . Black solid lines indicate the in-plane magnetic field. a) The out-of-plane Hall magnetic field, B_M . b) The in-plane electron velocities, $v_{e,L}$. c) Electron velocities in LN plane observed by MMS1-4 between 10:33:29.50 (bottom) and 10:33:30.60 (top). The solid and dashed lines mark the orientation of the magnetospheric and magnetosheath boundary, respectively. In this figure we have placed them at the limits of the electron outflow.

Crescent-shaped electron distributions

We observe crescent-shaped electron distributions in the electron outflow (Figure 4).

- The crescents constitute the peak jets within the electron outflow. The density decreases towards the magnetosheath, but the bulk velocity increases. The crescents are highly agyrotropic, but do not contribute to the agyrotropy of the total distributions, since the densities are too low (Figure 4a-c).
- The crescents form by a finite gyroradius effect occurring at the boundary between cold inflowing electrons and hot outflowing electrons, $T_{\perp,in} < T_{\perp,out}$. The heated electrons gyrate in the Hall magnetic field $B_M < 0$ (out-of-plane in Figure 4 \rightarrow counter-clockwise electron orbits) and extend toward the magnetosheath into the region with smaller T_{\perp} .
- The width of the outflow region $w \sim 15$ km is comparable to the gyroscales of the crescent electrons: $E_{max} = 180$ eV $\rightarrow \rho_e = 4.5$ km, indicating that the electrons are partly demagnetized and that their trajectories can extend outside the region with $B_M < 0$.
- Similar crescents have been observed in simulations [1,2], but primarily on the magnetospheric side of the X line, where they form due to meandering orbits of electrons crossing the neutral line. Following Bessho et al. 2016, we estimate the distance d to the Hall magnetic field neutral line $B_M = 0$:

$$v_{\perp 1} \geq \frac{v_{\perp 2}^2}{\omega_{ce} d} - \frac{\omega_{ce} d}{4} - \frac{|\mathbf{E} \times \mathbf{B}|}{B^2}. \quad (1)$$

The boundary provides a good cut-off, and we obtain $d = 1 - 7$ km (Figure 4g), which is comparable to the thickness of the outflow layer. The observed crescents are therefore consistent with meandering orbits.

Conclusions

We observe agyrotropic crescent-shaped electron distributions that form the peak jet in the narrow electron outflow of an asymmetric reconnecting current sheet. The crescents are formed by finite gyroradius effects toward the magnetosheath separatrix at the interface between cold inflowing electrons and heated outflowing electrons.

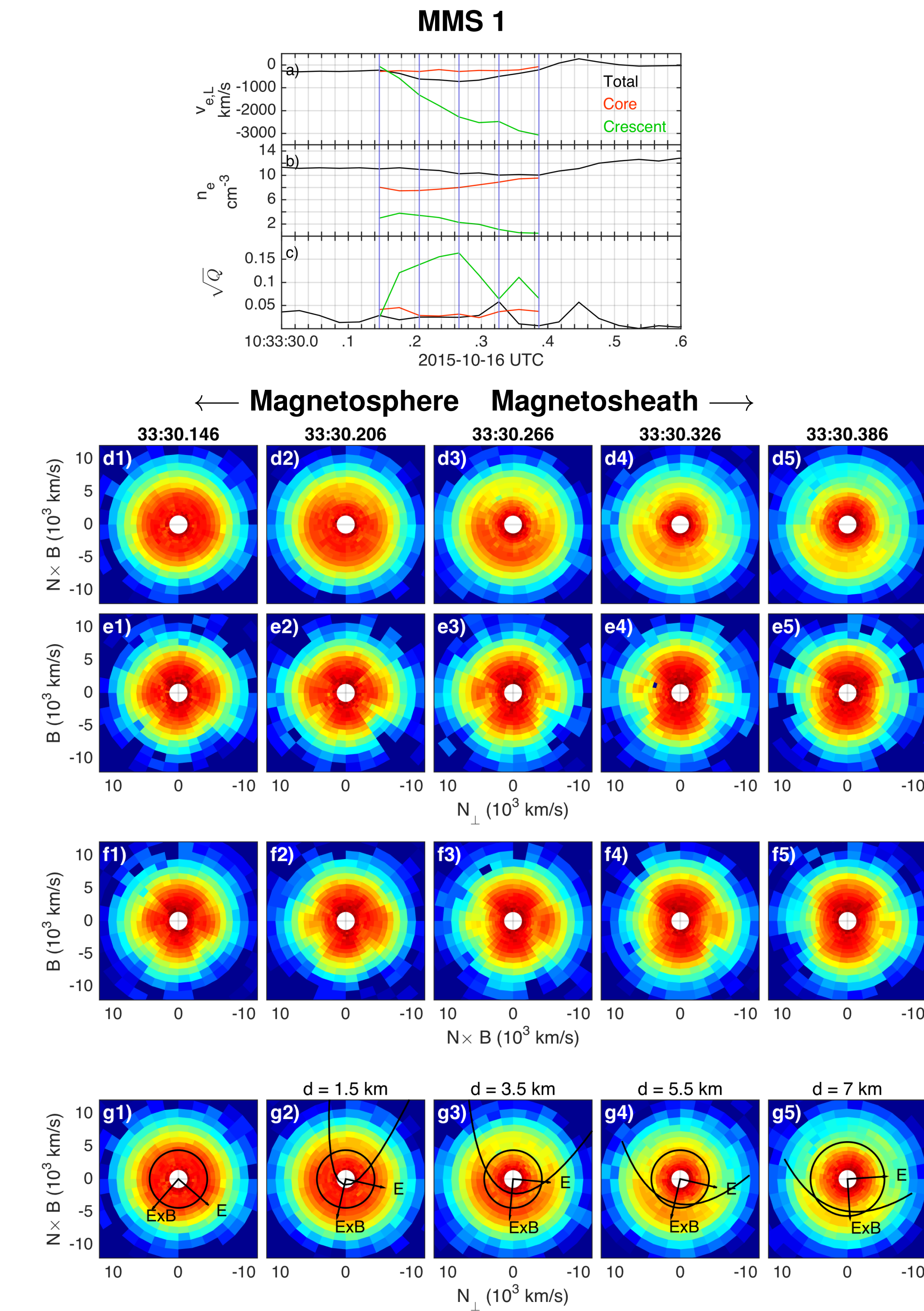


Figure 4: Properties and structure of electron phase space distributions observed by MMS1 in a thin current layer. a) Electron velocity $v_{e,L}$, b) density, and c) agyrotropy measure \sqrt{Q} for the total distribution, the core and the crescent, respectively. The vertical lines mark the times of the electron distributions shown in panels d-g. The projection of the electron distributions are made in planes perpendicular to; d) and g) \mathbf{B} , e) $\mathbf{N} \times \mathbf{B}$, and f) $\mathbf{N}_{\perp} = \mathbf{B} \times (\mathbf{N} \times \mathbf{B})$. Panel g) show the same plane as in d), but includes the local \mathbf{E} and $\mathbf{E} \times \mathbf{B}$ directions, as well as a fit to the lower bound of the crescents based on Eq. (1).

Acknowledgments

We thank the EDP, FPI, and FGM teams for providing excellent data! The data are available at <https://lasp.colorado.edu/mms/sdc/public>.

References

- Naoki Bessho, Li-Jen Chen, and Michael Hesse. Electron distribution functions in the diffusion region of asymmetric magnetic reconnection. *Geophysical Research Letters*, 2016. 2016GL067886.
- Li-Jen Chen, Michael Hesse, Shan Wang, Naoki Bessho, and William Daughton. Electron energization and structure of the diffusion region during asymmetric reconnection. *Geophysical Research Letters*, 2016. 2016GL068243.